AIChE

Conceptual Design of Distillation Processes for Mixtures with Distillation Boundaries. II. Optimization of Recycle Policies

Stefan Brüggermann
BASF SE, Verbund Structures Europe, D-67056 Ludwigshafen, Germany

Wolfgang Marquardt
Lehrstuhl für Prozesstechnik, RWTH Aachen, Turmstraße 46, D-52056 Aachen, Germany

DOI 10.1002/aic.12377
Published online August 23, 2010 in Wiley Online Library (wileyonlinelibrary.com).

Geometric design methods for the conceptual design of azeotropic distillation processes are fast and efficient tools for the economic screening of different process alternatives. The second article of this two-part series presents a novel optimization-based conceptual design framework for azeotropic distillation processes, which allows a rapid screening of the different process alternatives with respect to feasibility and economic incentive. The design framework is based on the economic assessment of distillation columns by the rectification body method. The feasibility limits imposed by the azeotropes are incorporated using the split feasibility test introduced in the first part of this series. The application of the framework is highlighted with several ternary and quaternary process alternatives for the production of high-purity alcohols. © 2010 American Institute of Chemical Engineers *AIChE J,* 57: 1540–1556, 2011
Keywords: design (process simulation), distillation, mathematical modeling, process synthesis, optimization

Introduction

Many azeotropic mixtures exhibit distillation boundaries that limit the reachable products of simple distillation columns.[1] Such mixtures cannot be separated by a sequential series of columns. Instead, processes in which the columns are coupled by one or more recycle streams must be utilized. Usually, there are several competing design alternatives. A typical example is the purification of an alcohol–water mixture. Because of the recycle streams, the mass balances of each of these processes are characterized by one or more degrees of freedom. To rate the economic potential of any of these alternatives in the conceptual design phase, the respective degrees of freedom have to be optimized with respect to a suitable cost definition. However, the limitation of the splits by the distillation boundaries is a major obstacle to the formulation of the optimization model as long as information about the distillation boundaries is only available implicitly, e.g., as a visualization of the residue curve map. The feasibility of a proposed process is then subject to a graphical analysis, which can hardly be automated. Therefore, the optimization problem cannot be solved using any standard numerical algorithm. Instead, several authors[2,3] propose methods to rank the importance of the optimization variables and then perform several one-dimensional sensitivity analysis steps to find the optimal solution. It can easily be imagined that this is a relatively time-consuming and tedious operation. Because of the limitations of visualization, such methods are further limited to ternary mixtures. Recent publications present algorithmic strategies to overcome this

Correspondence concerning this article should be addressed to W. Marquardt at wolfgang.marquardt@avt.rwth-aachen.de.

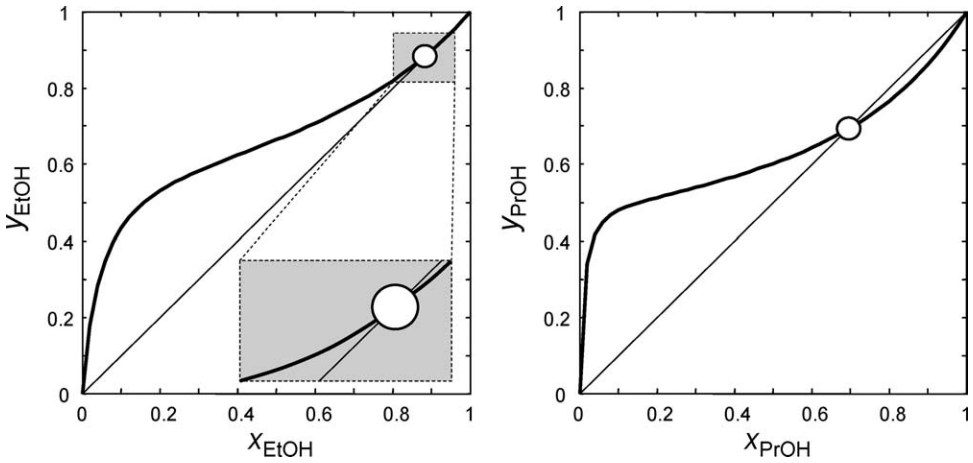

Figure 1. Vapor–liquid equilibrium of the ethanol–water (left) and the iso-propanol–water (right) mixtures in *x-y*-diagrams at atmospheric pressure.

limitation. A sequence of papers by Lucia and coworkers proposes geometric-based methods with optimization formulations for calculating exact separation boundaries.[4–7] These formulations are combined with minimum reflux calculation based on the concept of stripping line distance.[8,9]

In this article, a novel design framework for finding the optimal operating point of an azeotropic separation process is proposed. The design framework is based on the idea to use modern shortcut design methods to obtain a coarse approximation of the expected operating cost of any given process alternative quickly and with minimum effort. It incorporates the computational feasibility algorithm presented in the first article of this series. Because of the dispense of any graphical analysis, it allows to drop many limitations regarding the number of components and the complexity of the process alternatives. The operating point of a fixed flowsheet structure can thus be optimized with respect to all of its degrees of freedom simultaneously.

Illustrative Example: Purification of Alcohols

The purification of alcohols from an aqueous mixture is a classical example for the processing of azeotropic mixtures. Although being a fairly well-known separation task, it is still of significant industrial relevance. Especially, the cost-efficient production of high-purity ethanol has gained renewed importance recently because of the trend toward using ethanol as a fuel additive. The purification of alcohols is also a rewarding example for process design because many different process alternatives are known. In the following, some process alternatives for the separation of binary ethanol–water and iso-propanol–water mixtures will be introduced. They serve as illustrative examples for the application of the new design method. The discussion is limited to the two binary mixtures to be able to use binary and ternary phase diagrams for visualization. Some quaternary case studies of alcohol purification will be presented as additional examples.

Mixtures of either ethanol or iso-propanol and water form minimum boiling azeotropes at high concentrations of alcohol. Figure 1 shows the respective x-y diagrams at atmospheric pressure. Furthermore, the diagrams show that distillation close to the azeotrope on the water-rich side is limited by a tangent azeotrope. In terms of thermodynamics, both mixtures thus have a relatively similar behavior. Figure 2 shows six process alternatives based on distillation that, among others, can be applied for the alcohol purification. They can be categorized as pure distillation processes (alternatives a–c) and hybrid processes (alternatives d–f) that combine the distillation driving force between liquid and vapour composition with another physical phenomenon. For the sake of brevity, the following discussion of the alternatives will be limited to the purification of ethanol using the pure distillation processes shown in Figures 2a–c. However, it is important to note that all alternatives can be equally applied to the purification of iso-propanol as well. A more detailed discussion of separation options for alcohol–water mixtures including extractive distillation (Figure 2d) and heterogeneous distillation (Figure 2e) with various entrainers as well as distillation-membrane hybrid processes (Figure 2f) can be found elsewhere.[10,11]

The pressure-swing distillation process (see Figure 2a) uses the strong pressure-sensitivity of the ethanol–water azeotrope to promote the separation.[12,13] There are two variations of the process, namely the conventional and the entrainer-enhanced pressure-swing process. The conventional binary process is illustrated schematically in Figure 3 (left). The fresh feed *F* is mixed with the recycle stream *D2* from the second column to form the feed stream *M1* to the first column. This column is usually operated at atmospheric pressure. As *M1* lies to the left of the azeotrope at pressure p_1, high-purity water can be removed at the bottom (stream *B1*). A mixture close to the azeotrope is obtained as the distillate product *D1*. It is pressurized and then fed to the second column which is operated at a higher pressure, e.g., $p_2 = 10$ atm. As *D1* now lies to the right of the azeotrope at the elevated pressure, high-purity ethanol can be removed at the bottom of column 2 (stream *B2*), whereas the distillate product *D2* is recycled to the first column.

From a qualitative mass balance perspective, a small recycle flow rate *D2* is desirable for economic operation of the process. Thus, the distillate products of the pressure-swing process should be chosen as close to the respective azeotropes as possible. It can be inferred from the *T-x-y*

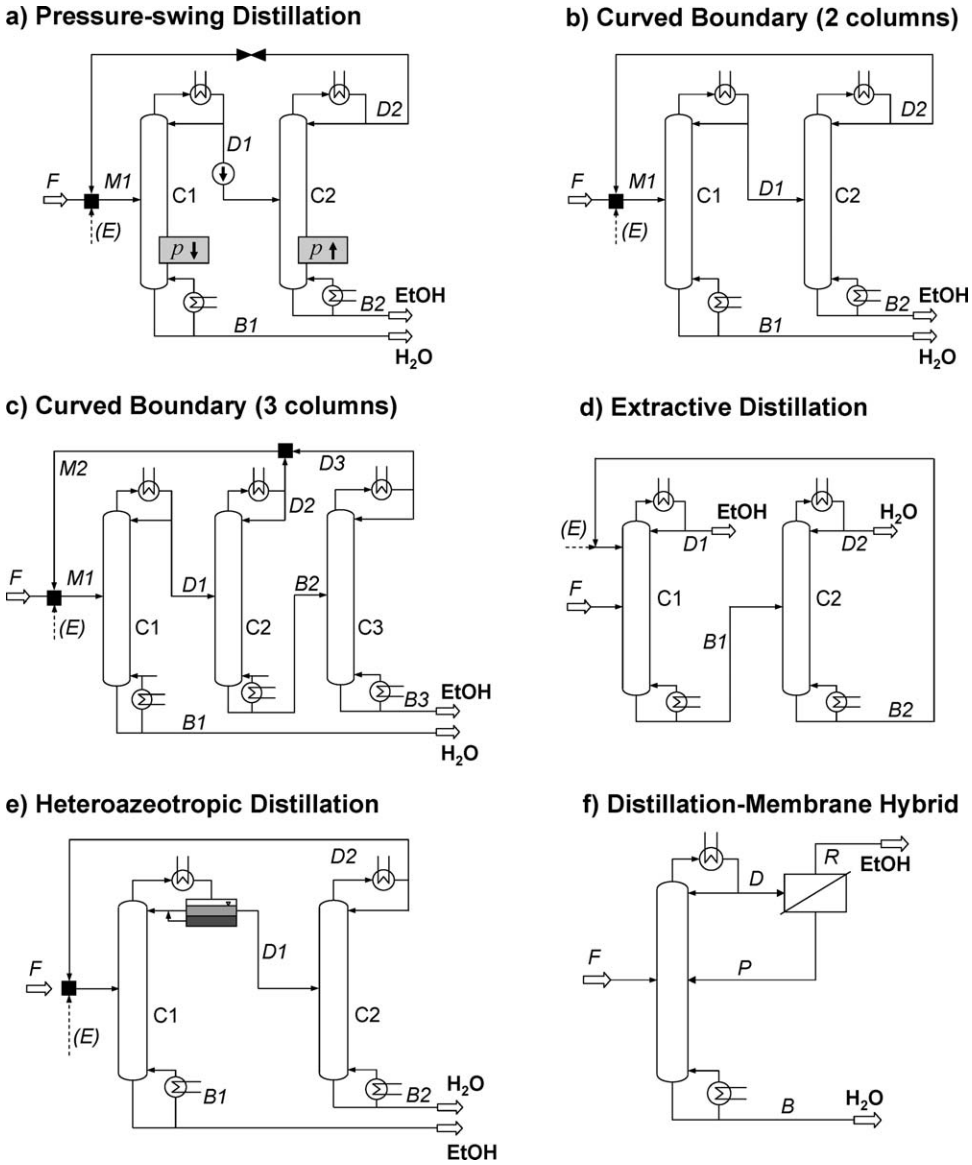

Figure 2. Process alternatives for the purification of ethanol or iso-propanol.

diagram in Figure 3 (left) that placement of *D1* close to the azeotrope will result in a severe limitation of the driving force in column 1 by the tangent azeotrope and thus in increased operating cost. The effect of this tangent azeotrope can be somewhat mitigated by the presence of a suitable entrainer, e.g., acetone. Therefore, Knapp and Doherty[2] propose an entrainer-enhanced ternary pressure-swing process (see Figure 3, right). The presence of the entrainer moves the compositions $\mathbf{x}_{D1}$ and $\mathbf{x}_{D2}$ of the distillate products *D1* and *D2* into the ternary region. At $p_2 = 10$ atm, one ternary azeotrope and three binary azeotropes, one on each binary edge, are found which separate the composition space into three distillation regions. The shaded area in Figure 3 (right) marks the feasible composition space for placement of $\mathbf{x}_{D1}$ and $\mathbf{x}_{D2}$ as predicted by the residue curves.

Comparing the two variations of the pressure-swing process, it is important to note that the complexity of choosing a good operating point increases dramatically by the introduction of the entrainer. The conventional process has two degrees of freedom on the flowsheet level, namely the compositions $x_{D1,EtOH}$ and $x_{D2,EtOH}$. Using the information from the *T*-*x*-*y*-diagram that the high pressure split is not subject to vanishing driving force close to the tangent azeotrope (cf. Figure 3, left), $\mathbf{x}_{D2}$ can be placed close to the azeotrope. Therefore, the optimal operating point can be found by a one-dimensional search in $x_{D1,EtOH}$. For the entrainer-enhanced ternary process, three degrees of freedom are observed, which are denoted by the thick open arrows in Figure 3 (right). Because of the lack of additional graphical information, it is not possible to reduce the amount of the degrees of freedom a-priori.

The curved boundary process (see Figures 2b, c) builds on the idea that a heavily curved distillation boundary can be overcome from its convex side by applying a clever combination of separation and mixing. To apply this process to the purification of ethanol, a suitable entrainer leading to the formation of the curved boundary is required. Stichlmair and Fair[14] propose the addition of tetrahydrofuran (THF), which

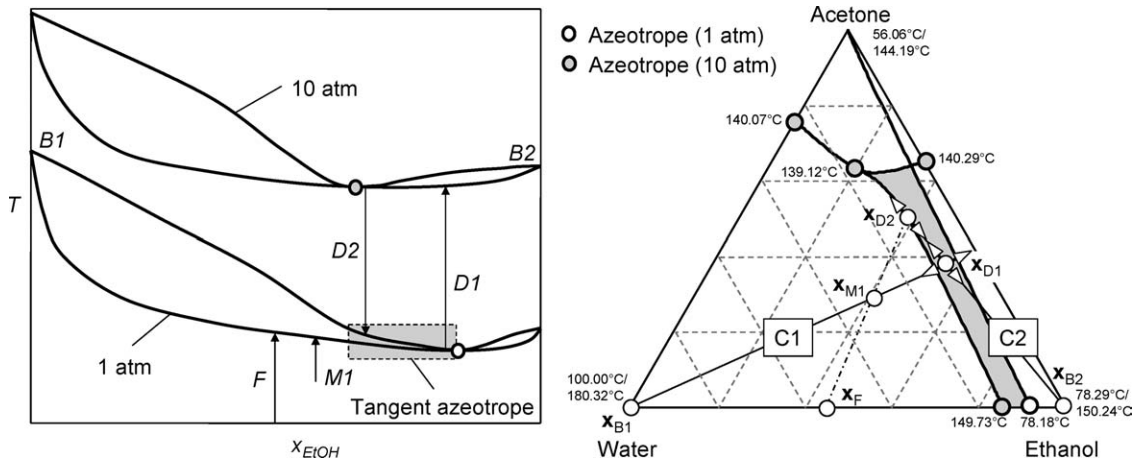

Figure 3. Graphical construction of the conventional (left) and the entrainer-enhanced (right) pressure swing processes.

Note that the *T-x-y* diagram (left) has been scaled for better legibility.

leads to the formation of two additional azeotropes. High-purity ethanol can then be obtained using a two-column process that has already been discussed in the first article of this series (cf. Figure 1 in first part of this series). The flowsheet is similar in structure to the pressure swing process. It is, therefore, not surprising to find that its operating point is also characterized by three degrees of freedom on the flowsheet level.

Widagdo and Seider[15] suggest to use methanol as the entrainer. No additional azeotropes are formed, and thus, the topology of the mixture is characterized by one single distillation boundary, which runs from the binary ethanol–water azeotrope to the methanol pure component vertex (see Figure 4). Two variations of the curved boundary process can be applied for this topology. In the first variation of the curved boundary process, the first split is specified such that water is obtained in the bottom product *B1*, and the distillate product *D1* is located close to the convex part of the boundary (see Figure 4, left). The second split then allows to move over to the other distillation region and obtain a binary mixture, which is rich in ethanol in the bottom product *B2*. This mixture is further purified in the third column, and the ethanol is removed in stream *B3*. The two intermediate cuts *D2*, which is rich in methanol, and *D3*, which is a nearly azeotropic ethanol–water mixture, are recycled to column 1. Because of the two recycle streams, $2C = 6$ degrees of freedom on the flowsheet level exist (D_1, $\mathbf{x}_{D1}$, D_2, $\mathbf{x}_{D2}$). However, some of these degrees of freedom can easily be eliminated by qualitative considerations with respect to the second column. It essentially describes a binary split of methanol and ethanol, which are known to separate easily. To get small recycle streams, it is, therefore, advisable to choose $\mathbf{x}_{D2}$ close to the pure methanol vertex and to place $\mathbf{x}_{B2}$ on the binary ethanol–water edge. Using these assumptions, only the two degrees of freedom on $\mathbf{x}_{D1}$ remain (cf. thick open arrows in Figure 4, left).

The second variation of the curved boundary process using methanol as the entrainer is based on the observation that the residue curve map predicts that the distillation boundary clings to the binary methanol–ethanol edge for

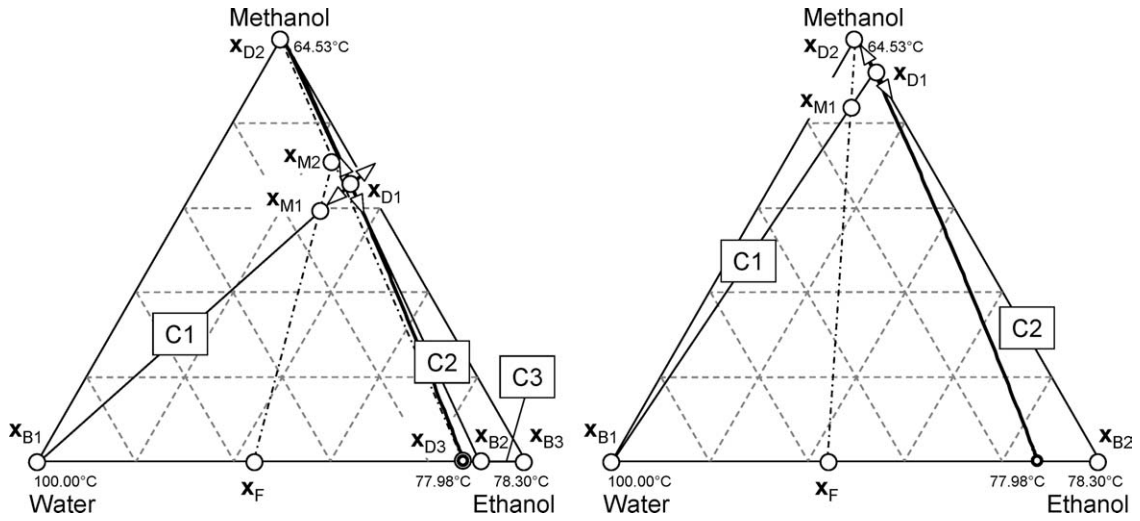

Figure 4. Curved boundary processes with three columns (left) and two columns (right) for the purification of ethanol using methanol as the light entrainer.

Table 1. Summary of Distillation-Based Process Alternatives with Respect to Entrainer, Number of Components C, Number of Columns N_{Col}, Additional Equipment and Design Degrees of Freedom N_{DF}

Process	Index	Entrainer	C	N_{Col}	Addtl. Equipment	N_{DF}
Pressure-swing	a)	–	2	2	–	1
		Acetone	3	2	–	3
Curved boundary	b)	THF	3	2	–	3
		Methanol	3	2	–	1
	c)	Methanol	3	3	–	2
Extractive distillation	d)	Ethylene glycol	3	2	–	1
Heteroazeotropic distillation	e)	Cyclohexane	3	2	Decanter	3
Pervaporation-Distillation	f)	–	2	1	Membrane	1

high methanol concentrations. If the distillate product of the first column *D1* is placed in that region, a high-purity ethanol product can be obtained in the second split (see Figure 4, right). Therefore, the process is reduced to two columns with one degree of freedom, which describes the placement of *D1* on the boundary. However, it can be inferred from the lever arm rule that this mode of operation requires a large recycle flow rate D_2.

Table 1 summarizes the technically relevant degrees of freedom on the flowsheet level for the six distillation-based process alternatives shown in Figure 2. Where applicable, the reduction of the degrees of freedom using insight from the thermodynamics of the respective mixture as discussed above has already been incorporated. It can be seen that even if only a limited number of components and units operations is involved, there are several alternatives that have more than one degree of freedom on the flowsheet level. It is obvious to expect this number to increase sharply for mixtures and flowsheets with increased complexity.

A New Process Design Framework Based on Shortcut Methods

The design framework is based on the idea to use modern shortcut design methods to obtain a coarse approximation of the expected operating cost of any given process alternative quickly and with minimum effort. In this respect, it shows some similarities to methods for cost targeting involving a manual analysis of distillation boundaries using residue curve maps.[2,3] A key characteristic is that the new framework aims at providing a fully algorithmic formulation of the optimization of the operating point by exploitation of the fully computational feasibility algorithm presented in the first article of this series. Because of the dispense of any graphical analysis, it allows to drop many limitations regarding the number of components and the complexity of the process alternatives in manual analysis. The operating point can thus be optimized with respect to all of its degrees of freedom simultaneously. First, a general formulation of the optimization model will be given. To use this formulation, an algorithmic procedure for the determination of the feasibility and the profitability of each occurring unit operation must be known.

In a given flowsheet structure, discrete decisions can only be found within the unit operations, such as the number of trays of a distillation column. On the flowsheet level, only continuous variables are found. For example, consider the two-column pressure-swing process shown in Figure 2a. Given the feed and product specifications and assuming for the moment that the pressures and the thermal states of all streams are fixed, the operating point of the flowsheet is completely described by the component flow rates $\mathbf{u} = (\mathbf{m}_1^T, \mathbf{d}_1^T, \mathbf{d}_2^T)^T$. The assumption regarding pressure and thermal state can be relaxed by adding pressures and enthalpies to the set of variables $\mathbf{u}$. The optimal operating point can be found by solving the nonlinear program

$$\min \Phi(\mathbf{u}) \tag{1}$$

$$\text{s.t.} \quad \mathbf{A}\mathbf{u} = \mathbf{b}, \tag{2}$$

$$g_i(\mathbf{u}) \le 0, \qquad i = 1, \ldots, N_{\text{unit}}, \tag{3}$$

$$h_k(\mathbf{u}) \le 0, \qquad k = 1, \ldots, N_{\text{opcon}}, \tag{4}$$

$$u_j \ge 0, \qquad j = 1, \ldots, V, \tag{5}$$

where N_{unit} is the number of units in the process, N_{opcon} is the number of operational constraints, and V is the number of variables in $\mathbf{u}$. Matrix $\mathbf{A}$ and vector $\mathbf{b}$ contain the mass balances of the flowsheet. The objective function Φ defines the basis for evaluation of the profitability of the operating point. Different formulations of Φ may be chosen depending on the required level of accuracy of the cost description. In the following, the discussion of profitability will be limited to the minimization of operating cost.

The minimization of the overall recycle flow rate gives a very coarse approximation of the expected operating cost. It is based on the perception that the energy demand of a column increases with the corresponding feed flow rate. As these flow rates increase with the flow rates of the recycle streams, a minimal separation effort can be expected, if the recycle streams are small. However, this formulation completely ignores that the energy demand of each column is not only affected by the amount of material that needs to be separated. It is also strongly influenced by the driving force of the separation which may change significantly with respect to the operating point. Although its accuracy is limited, it should be noted that this formulation has the interesting property that it does not require any profitability model. For the pressure-swing process in Figure 2a, for example, the minimization of the overall recycle flow rate corresponds to

$$\Phi_{\text{Rcy}} = \sum_{j=1}^{C} d_{2,j}. \tag{6}$$

The approximation of process cost by the minimum energy demand takes the influence of the vapor–liquid driving force on the operating cost of distillation processes into account. The rectification body method (RBM, see Bausa et al.[16]) is used to obtain the reboiler and condenser heat duties $(Q_{B,i}, Q_{D,i}) = \text{f}(\mathbf{u})$ for each column i. Usually, the cooling cost

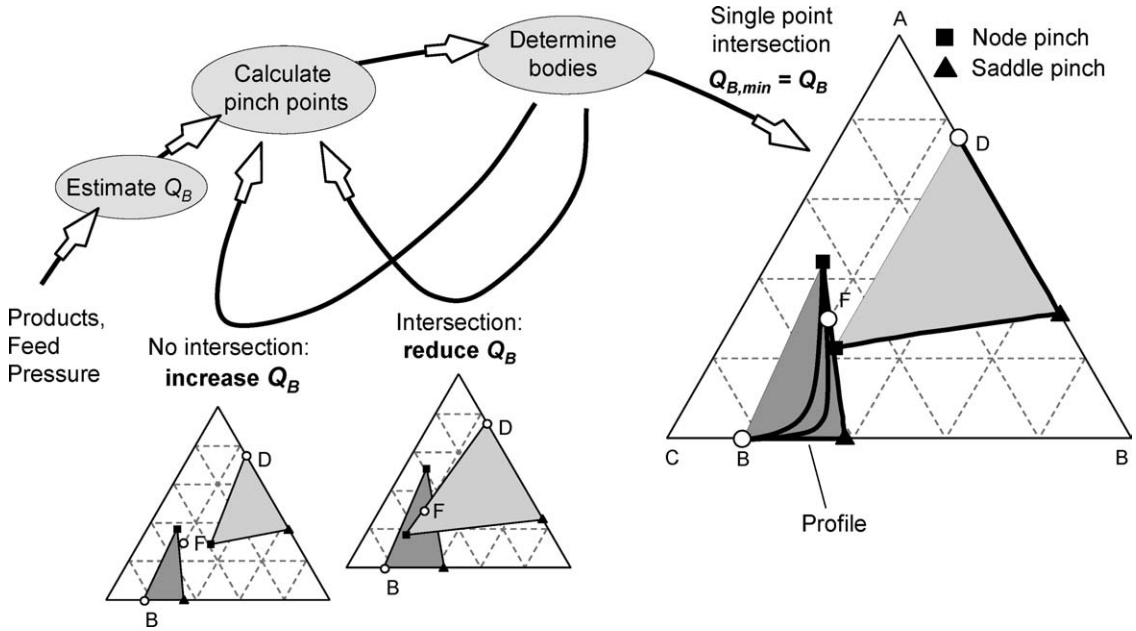

Figure 5. Structure of the RBM algorithm.

are assumed to be negligible compared to the cost for heating. The objective function can thus be formulated as

$$\Phi_{\mathrm{En}} = \sum_{i=1}^{N} Q_{\mathrm{B,i}}(\mathbf{u}). \tag{7}$$

This formulation can be expected to give a good account of the energetic performance of the process within the accuracy provided by the RBM. It should be noted, however, that a minimization of the reboiler energies does not take into account at which temperature the heating has to be provided.

The linear constraints in Eq. 2 are introduced to enforce the mass balances around each unit of the process. If applicable, they also contain the energy balances and the pressure relations between the streams. For the pressure-swing process in Figure 2a with fixed thermal states and pressure levels, the balance equations

$$m_{1,j} - d_{1,j} = b_{1,j}, \quad j = 1,...,C, \tag{8}$$

$$d_{1,j} - d_{2,j} = b_{2,j}, \quad j = 1,...,C, \tag{9}$$

around the two columns are sufficient. It should be noted that the balances around the mixer can be omitted because they are linearly dependent and thus provide no additional information.

The limitation of the splits by feasibility boundaries, e.g., distillation boundaries, is modeled by the nonlinear inequality constraints in Eq. 3. In the following, these constraints will be termed feasibility constraints. Their formulation will be based on the determination of distillation boundaries as presented in the first article of this series. The additional set of nonlinear constraints in Eq. 4 can be used to enforce additional operational considerations as set forth by the user. Examples for such operational constraints can be the enforcement of a minimum distance of the operating point from a feasibility boundary or the introduction of bounds on the temperature of some stream to be able to use it for heat integration. Finally, Eq. 5 guarantees positive flow rates.

Determination of the Minimum Energy Demand

Although shortcut methods for the determination of the minimum energy demand of the distillation of ideal mixtures have been widely used for many years,[17] approximative design methods capable of analyzing nonideal azeotropic mixtures have a much younger history. The boundary value method (BVM) of Levy et al.[18] marks one of the early breakthroughs. It is based on the calculation of tray-by-tray profiles by iteratively solving the mass and energy balance equations from plate to plate. For a set of product specifications, such as the distillate flow rate D, the composition $\mathbf{x}_{\mathrm{D}}$ and the enthalpy h_{D}, and for given column pressure p and condenser heat duty Q_{D}, these profiles can be obtained using an implicit recursion of the form

$$\left(\mathbf{x}_{n+1}, \mathbf{y}_{n+1}, T_{n+1}, V_{n+1}, L_n\right) = f(\mathbf{x}_n, D, \mathbf{x}_{\mathrm{D}}, h_{\mathrm{D}}, p, Q_{\mathrm{D}}), \tag{10}$$

for the rectifying section, and, similarly for the bottoms section.

Starting this calculation from the distillate and bottoms product, respectively, the profiles of the rectifying and the stripping section are determined. For a feasible column, these profiles must intersect. However, a rather strong sensitivity of the course of the profiles with respect to this choice of trace components in the distillate and bottoms products is observed. For example, the large ternary diagram on the right hand side of Figure 5 shows three significantly different stripping section profiles which can be obtained by changing the amount of component A in the sub-ppb-range. This sensitivity with respect to trace compositions in the products represents a drawback for the determination of the minimum reflux by tray-by-tray design (for a more complete discussion see Bausa et al.[16]).

One way to decouple the determination of the minimum energy demand from the choice of the trace compositions is to ensure that only the most far-reaching profiles are checked for intersection. The pinch points provide useful information

to reliably find these profiles. They describe the compositions on the profile where the vapor–liquid driving force of the separation vanishes. Mathematically, the pinch points can be interpreted as singular points of the implicit recursion in Eq. 10 for the calculation of the profiles. Therefore, they can be calculated for the rectifying section by solving

$$0 = V - L - D, \tag{11}$$

$$0 = Vy_i - Lx_i - Dx_{\mathrm{D},i}, \quad i = 1, \ldots, C, \tag{12}$$

$$0 = y_i - K_i(\mathbf{x}, \mathbf{y}, T, p)x_i, \quad i = 1, \ldots, C, \tag{13}$$

$$0 = \sum_{k=1}^{C} (y_k - x_k), \tag{14}$$

$$0 = Vh^V(\mathbf{y}, T, p) - Lh^L(\mathbf{x}, T, p) - Dh_{\mathrm{D}} + Q_{\mathrm{D}}. \tag{15}$$

The pinch points for the stripping section can be calculated analogously. As the column profiles themselves, the pinch points only depend on the heat duty, if the mass balance of the separation is fixed. However, it can be shown that pinch points are insensitive to the choice of the trace compositions. Often several pinch points can be found for each section. For example, the large ternary diagram in Figure 5 shows two pinch points for the rectifying and another two pinch points for the stripping section. The complete set of all pinch points as a function of Q_{D} and Q_{B}, respectively, can be reliably obtained using a homotopy continuation strategy starting from the product composition and all singular points of the residue curve map, i.e., azeotropes and pure components (see Bausa[19]). Furthermore, the course of the profiles close to the respective pinch point can be determined using the information contained in the eigenvalues and eigenvectors of the set of pinch equations 11–15 (see Julka and Doherty[20]). Correspondingly, the pinch points can be classified as unstable nodes, saddles and stable nodes.

The analysis of the course of column profiles and the types of pinch points allows to develop an understanding of the patterns in which a profile can potentially evolve. Bausa et al.[16] use this property for the development of the rectification body method (RBM). It is based on the construction of geometrical bodies based on the location of the pinch points which approximately describe the manifold of all profiles. Hence, the search for intersecting profiles can be replaced by looking for an intersection of the bodies. To calculate the minimum energy demand using the RBM, it is, therefore, sufficient to iteratively search for the lowest reboiler heat duty that results in a set of bodies that intersect. Figure 5 shows a graphical interpretation of the RBM algorithm. Starting from a set of given product specifications, feed specification and pressure and a first guess of the reboiler energy Q_{B}, the pinch branches and pinch points are calculated and the rectification bodies are formed. If there exists an intersection between a body of the rectifying section and one of the stripping section Q_{B} is decreased. Otherwise Q_{B} is increased. This process is continued until the minimum energy demand $Q_{\mathrm{B,min}}$, i.e., the reboiler heat duty which cannot be reduced without losing intersection, is found within the desired tolerance.

Note that this algorithm has several favorable properties. First, it is based on pinch information and, therefore, is not affected by trace compositions. Second, it is not limited to specific types of splits because it makes use of all pinch points. Finally, the check for intersection of the bodies can be fully automated and, therefore, there exists no limitation on the number of components of the mixture. For more complex mixtures, more than one body for each section may exist. Each body may take any dimensionality from a simple line to a polyhedron in C-1 dimensions. Details on the algorithmic approach of the RBM and its properties, e.g., the way it deals with the feed mismatching phenomenon frequently encountered in tray-by-tray calculation, can be found in Bausa et al.[16]

Several authors propose alternative methods for finding the minimum energy demand based on the set of all pinch points. Most of these methods use empirical or semiempirical criteria to decide on which pinch points need to be considered. The zero-volume criterion (ZVC; Julka and Doherty[20]), the minimum angle criterion (MAC; Köhler et al.[21]), and eigenvalue criterion (EC; Pöllmann et al.[22]) are some of the best known methods. However, most of these methods are limited either by the types of splits or by the number of components. Recent strategies, such as the determination of the shortest stripping line distance,[8,9] are able to overcome some of the limitations.

Application of the Design Framework to the Optimization of the Recycle Policy

The first step for the optimization of the operating point of a process alternative is the formulation of the constraints and the objective function which are given in abstract terms by Eqs. 1–5. To make the approach easier to grasp, it will now be set up for the dehydration of ethanol in a ternary entrainer-enhanced pressure-swing process (cf. flowsheet in Figure 2a). The model of the process has $3C$ unknown variables $\mathbf{u} = (\mathbf{m}_1^T, \mathbf{d}_1^T, \mathbf{d}_2^T)^T$ and $2C$ linearly independent balance equations around the two columns. Hence, the process is characterized by C degrees of freedom which are to be optimized (see Figure 3, right).

For the time being, the minimization of the energy demand of the process given by the cumulative reboiler heat demand (cf. Eq. 7) is aimed at. The optimization model is then given by

$$\min \Phi_{\mathrm{En}}(\mathbf{u}) = Q_{B1,\min}(\mathbf{u}) + Q_{B2,\min}(\mathbf{u}) \tag{16}$$

$$\text{s.t} \quad m_{1,i} - d_{1,i} = b_{1,i}, \qquad i = 1, \ldots, C, \tag{17}$$

$$d_{1,i} - d_{2,i} = b_{2,i}, \qquad i = 1, \ldots, C, \tag{18}$$

$$m_1(\mathbf{u}) \geq 1, \tag{19}$$

$$m_2(\mathbf{u}) \geq 1, \tag{20}$$

$$u_j \geq 0, \qquad j = 1, \ldots, 3C. \tag{21}$$

The linear Eqs. 17 and 18 model the mass balances around the columns. Every time the constraints are evaluated, each of the feasibility constraints in Eqs. 19 and 20 triggers a subordinated homotopy continuation that returns the respective value of m_1 or m_2 as a function of $\mathbf{u}$ where m_1 and m_2 correspond to the observation of the distillation boundaries by the splits in columns 1 and 2, respectively. Equation 21 assures the non-negativity of any component flow rate.

Table 2. Stream Table for the Ternary Pressure-Swing Process at the Energetically Optimal Operating Point

Flow rate (kmol/s)	F	M1	D1	B1	D2	B2
Acetone	0.000	0.062	0.062	0.000	0.062	0.000
Ethanol	0.042	0.070	0.070	0.000	0.028	0.042
Water	0.958	0.967	0.009	0.958	0.009	0.000
Total	1.000	1.099	0.141	0.958	0.099	0.042

A feed flow rate of $F = 1$ kmol/s with 4.2 mole % ethanol is assumed. Furthermore, the following additional assumptions were made:

(1) Pressure-change equipment, e.g., pumps, valves, compressors, and turbines, are not modeled.

(2) All products of the two columns are withdrawn as saturated liquids.

(3) All feed streams, i.e., *M1* and *D1*, are supplied to the columns as saturated liquids at the column pressure.

In principle, assumption 3 violates the energy balances around the mixer and the pump (cf. Figure 2a) because in both cases a small amount of heating would be necessary to achieve the desired properties of the feed streams. However, the influence of the assumption on the overall energy demand has been found to be negligible because the missing heat streams do not involve phase change and, therefore, are several orders of magnitude lower than the reboiler and condenser duties. In the context of a conceptual screening of the process, it consequently makes sense to waive the modeling of the energy balances in favor of keeping the optimization model compact.

Because of the compact form of the model in Eqs. 16–21, the optimization is very robust and converges for an arbitrary initialization of the vector of the variables **u**. Several initializations were tried. For all performance data of the optimization given below, all entries of **u** were initialized by setting them to unity. This initialization is infeasible with respect to both the linear mass balances as well as the nonlinear feasibility constraints. With the standard set of computational parameters of the used nonlinear solver CFSQP,[23] the optimization converges after 28 iterations. The computation time is ~6 min on a fairly outdated PC with an AMD Athlon XP 2200+ CPU. Some adjustments of the parameters allow to reduce the required computation time down to about 2 min. Additional details on the computational performance have been reported by Brüggemann.[10]

Using the assumptions stated above, the optimization of Eqs. 16–21 yields a minimum overall reboiler heat duty $Q_{BT,min} = 32.3$ MW, where $Q_{B1,min} = 18.9$ MW and $Q_{B2,min} = 13.4$ MW. The component flow rates at this operating point as obtained from **u** are given in Table 2. Figure 6 presents a visualization of the mass balances of the process in a ternary diagram. The figure also includes a sketch of the flowsheet without pressure change devices for easy reference. It can be seen that the distillate composition $\mathbf{x}_{D2}$ of the second column is located at the point of intersection of the two PDB originating from the ethanol–water and the acetone–ethanol azeotropes. Hence, the maximum distance to the pure ethanol vertex in the solid-shaded pressure-swing area is attained. Correspondingly, only a small flow rate D_2 of the recycle stream is required according to the lever arm rule. Contrarily, the distillate composition $\mathbf{x}_{D1}$ of the first split is not placed on the PDB at atmospheric pressure, even though this situation would again be favorable with respect to the lever arms. Instead, it is somewhat shifted toward the pure water vertex.

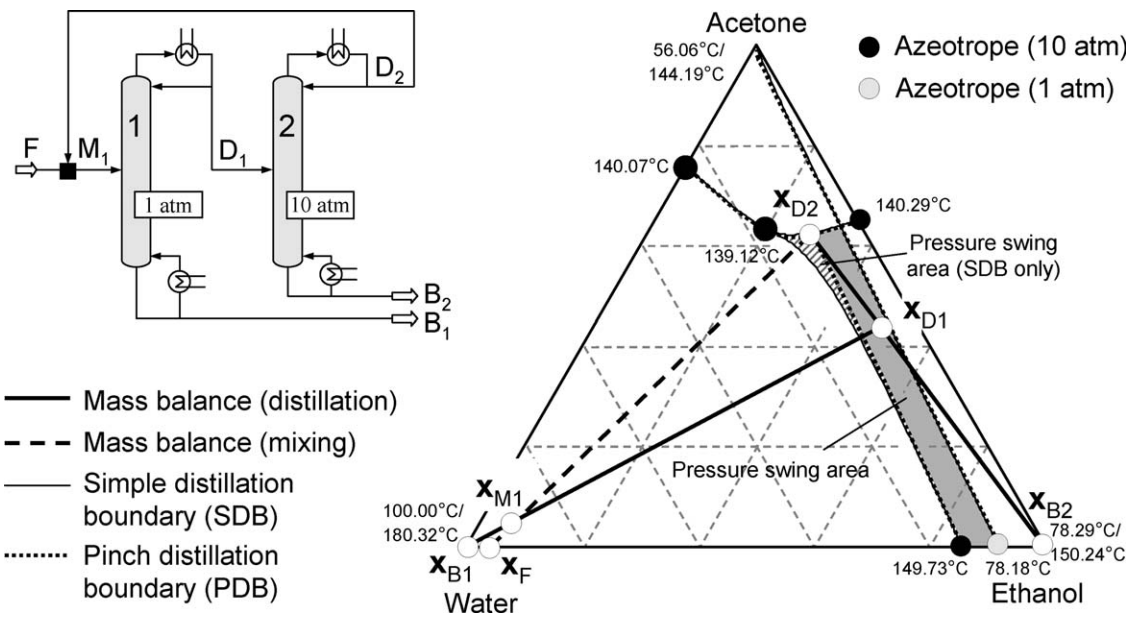

Figure 6. Mass balances of the ternary pressure-swing process at the energetically optimal operating point.

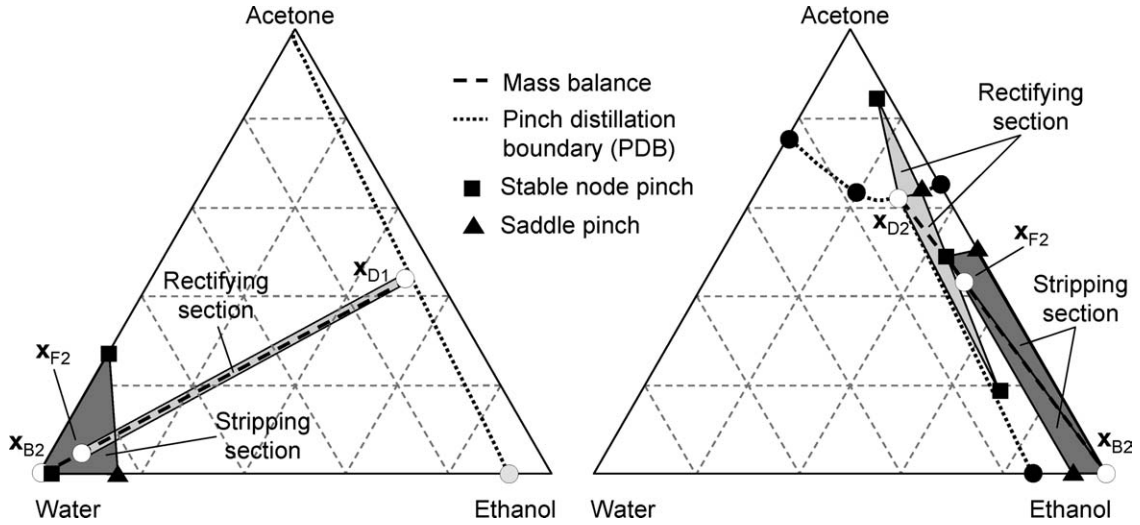

Figure 7. Rectification bodies of the low-pressure column (left) and the high-pressure column (right) at optimal operating point and minimum energy demand.

Figure 7 shows the rectification bodies for both columns. For the rectifying section of the low-pressure column, only one stable node pinch is found. Hence, a linear rectification body results which almost coincides with the mass balance line. It can be seen that this linear body largely overlaps the triangular rectification body of the stripping section. This behavior refers to the appearance of a tangent pinch. The effect of the tangent pinch increases sharply when the PDB is approached. Hence, the elevated energy demand due to the tangent pinch causes the placement of $\mathbf{x}_{D1}$ in some distance to the PDB. The tangent pinch phenomenon does not occur in the ethanol-rich distillation region where the split in the high-pressure column is located.

Knapp and Doherty[2] discuss the design of the same example process using the BVM. While they do not state the number of trays of both columns explicitly, it can be deduced from their graphs that it is fairly large (>50 for each column section). Therefore, they also operate the columns close to minimum reflux so that their results can be directly compared to the ones obtained from the new optimization-based design framework. They report a slightly lower overall energy demand $Q_{BT,min} = 30.6$ MW where $Q_{B1,min} = 16.1$ MW and $Q_{B2,min} = 14.5$ MW. Hence, their design is superior by 5.2%. The corresponding operating point is illustrated in a ternary diagram in Figure 8.

It can be seen that their choice of $\mathbf{x}_{D2}$ is located in the gusset of the SDB and the ternary azeotrope. The difference in the overall minimum energy demand and the operating point between the optimization based on PDB and RBM and the literature source can be attributed to the different methods for the feasibility analysis of the two design approaches. The following section provides a more detailed analysis. For

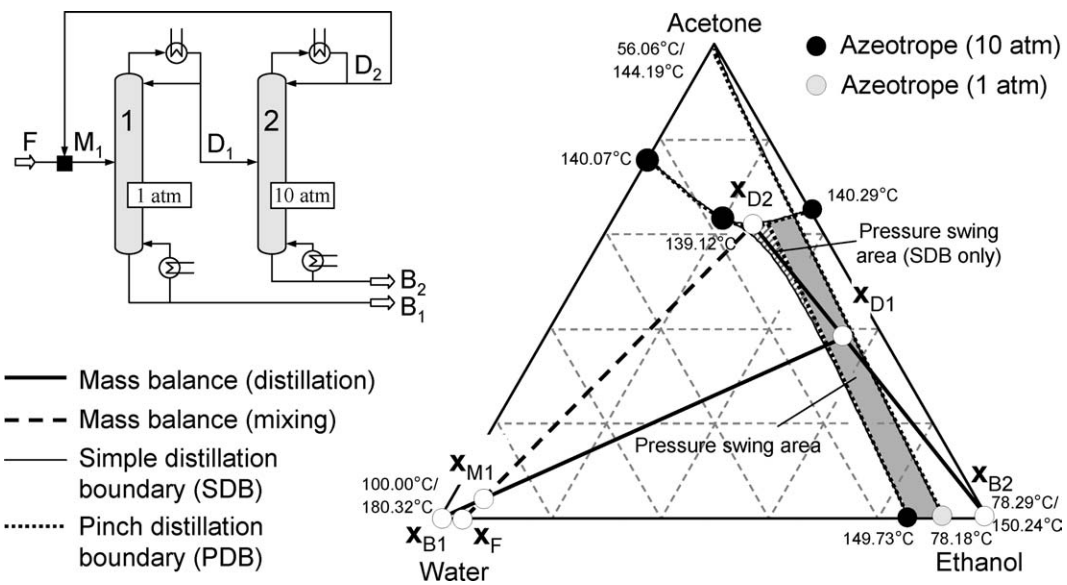

Figure 8. Optimal operating point from literature (Knapp and Doherty[2]).

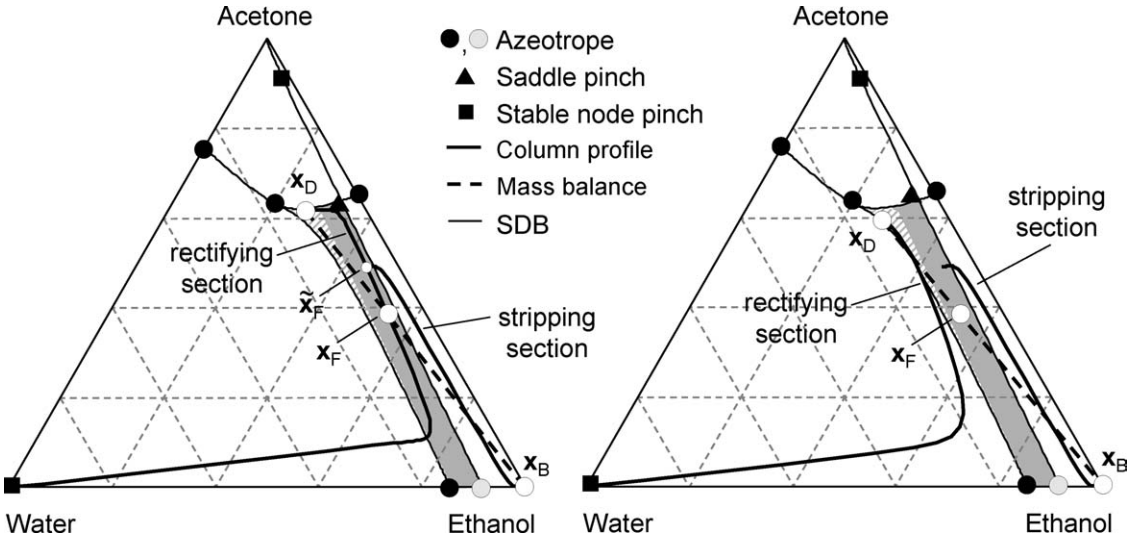

Figure 9. Column profiles of the high-pressure column for the feasible product specifications taken from Knapp and Doherty[2] (left) and for an infeasible set of product specifications obtained by a small variation of $x_{D,Acetone}$ (right).

the conceptual screening of process alternatives, which is still subject to a large array of uncertainties, however, small variations of 5% in the objective of the optimization can be tolerated. Simulation of this process with AspenPlus shows that the operating point found from the conceptual optimization can be reproduced qualitatively.[10]

It should be noted that the pressure-swing process as illustrated in Figure 2a and discussed above represents a base case. Several improvements of this base case process are conceivable. For example, the distillate stream *D2* of the high-pressure column can be drawn off as vapor. Hence, the condenser duty Q_{D2} is reduced and, as an additional positive effect, the heat of condensation of *D2* can be used to heat up the feed stream *F* in the mixer unit. The replacement of the valve with a turbine yields a second opportunity for improvement by using the pressure drop for the generation of mechanical or electrical energy. For example, this energy could be used to propel the pump which pressurizes stream *D1*. However, an analysis of the results of the base case process shows that the amount of reboiler energy that can be saved using these improvements is very small. Hence, they do not need to be considered in the context of a rough conceptual screening. However, they should be revisited at a later, more detailed stage of analysis. In contrast to the modifications discussed above, a significant economic improvement can be expected from heat integration within the process.[10,24] The minimum driving force for heat integration and the temperature-dependency of steam cost also drive the selection of the operating pressure p_2 of the high-pressure column.

Properties and Limitations of Pinch-Based Design

Comparing Figures 6 and 8, it can be seen that both operating points look qualitatively similar. However, the design by Knapp and Doherty[2] places $\mathbf{x}_{D2}$ inside the shaded pressure swing area where the feasibility assessments given by the SDB used by them and the PDB contradict. In this region, the feasibility of the split is a function of the reflux ratio (cf. first part of this series). Knapp and Doherty[2] confirm the feasibility of their design using tray-by-tray calculations. The slightly more energy-efficient performance of their process can be attributed to the specific choice of $\mathbf{x}_{D2}$ in a distillation region that is not accessible to the optimization based on RBM and PDB.

To gain some insight into the properties of the corresponding split in the high-pressure column, an analysis of the tray-by-tray profiles of high-pressure column is performed. Figure 9 (left) shows the respective column profile of the rectifying section together with the pinch branches. It can be seen that a large portion of the profile runs within the ethanol rich pinch distillation region before turning toward the water vertex. It intersects with the corresponding stripping profile at the feed tray composition $\tilde{\mathbf{x}}_F$ within this region. However, the situation changes completely if $\mathbf{x}_D$ contains 1 mole % less acetone (Figure 9, right). Note that this composition is still located within the striped SDB pressure-swing area. For the same condenser heat duty Q_D, the profile leaves the pressure-swing area very quickly. An intersection with a profile of the stripping section cannot be found. Hence, the split is infeasible for this value of Q_D. An iterative search further shows that feasibility can only be achieved for very high values of Q_D, i.e., close to infinite reflux.

In addition to violating the PDB-based feasibility test, the high-pressure split by Knapp and Doherty[2] also bears problems for the application of pinch-based methods for the determination of the minimum energy demand. Figure 10 shows the pinch map of the rectifying section for $\mathbf{x}_D$ in both ternary diagrams and as a function of the reflux ratio *r*. In the left ternary diagram pinch points, eigenvectors, rectification bodies and profiles of the rectifying section are given for $r = 5.8$ (as in Knapp and Doherty[2]). Two rectification bodies are found. The lower one corresponds to the profile. It can be seen that the body does not describe the path of the profile at all. Most strikingly, there is a large discrepancy between the body and the local behavior of the profile close

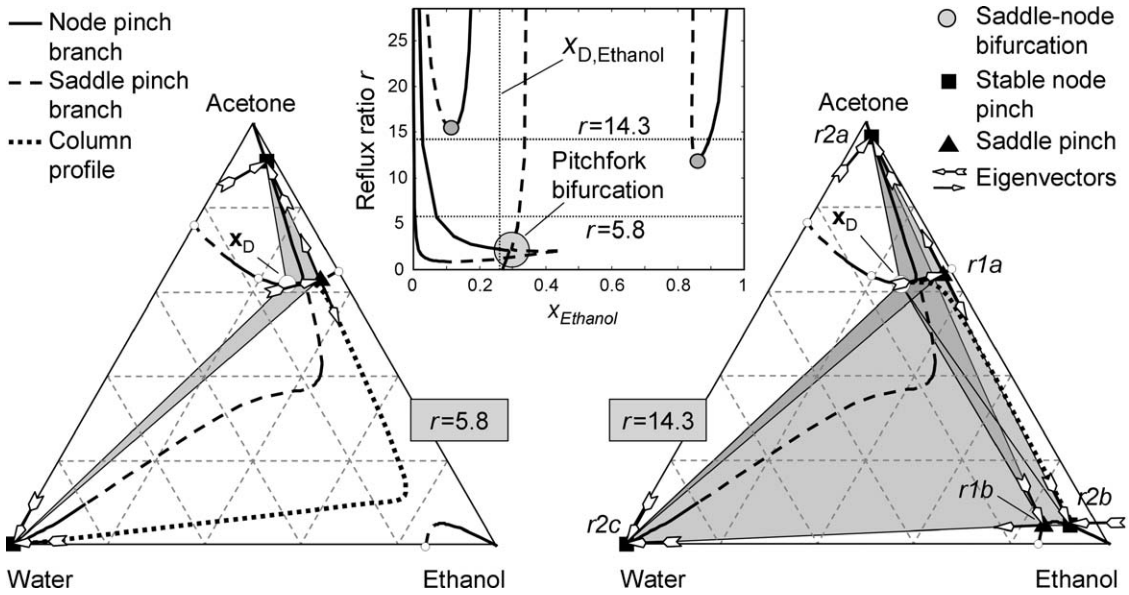

Figure 10. Pinch map of the rectifying section of the high-pressure column for the feasible product specifications taken from Knapp and Doherty[2].

Pinch points, eigenvectors, rectification bodies and profiles of the rectifying section at $r = 5.8$ (left) and $r = 14.3$ (right).

to the saddle and node pinch points as given by the eigenvectors. Because of the poor approximation of the profile by the body, the reflux ratio is, hence, incorrectly rated insufficient by the RBM.

For this split, an intersection of the bodies of the rectifying and stripping section can only be obtained if r is increased above the reflux ratio $r_{SN} = 12.0$ of the saddle-node bifurcation shown in the upper right part of the reflux diagram. In this case, additional pinch points on the pinch branches between the ethanol–water azeotrope and the ethanol vertex are found. The right ternary diagram in Figure 10 shows the respective rectification bodies of the rectifying section. It can be seen that the profile is well-described by the body connecting $\mathbf{x}_D$, *r1a* and *r2b*. Because of the large number of pinch points, however, a large number of additional bodies is found. Most of them, e.g., the one connecting $\mathbf{x}_D$, *r1b* and *r2a*, are of no physical significance. While these bodies do not contribute to the determination of the minimum energy demand in this specific example, they can potentially lead to incorrect conclusions in other cases. Hence, the application of pinch-based methods for the determination of the minimum energy demand like RBM is not recommended for product compositions outside the pinch distillation region of the split.

Additional Examples

This section presents some illustrative examples for the application of conceptual process optimization using the new design framework. The design of a process for the separation of a mixture with a curved distillation boundary using two different objective functions is discussed. A quaternary curved boundary process demonstrates the applicability of the approach to mixtures with more than three components. Finally, a second quaternary example highlights how insight from the analysis of the PDB can be used for improving the sequencing of columns.

Ternary curved boundary process

For the curved boundary process with three columns, the operating point is characterized by $2C$ degrees of freedom (cf. Figures 2c and 4, left). The product streams *B1* and *B3* are fixed according to the global mass balance. The other streams are constrained by the mass balances around the three columns. The two subsequent mixing operations are aggregated into one mixing unit with three input streams. Hence, stream *M2* is not included in the set of variables $\mathbf{u} = (\mathbf{m}_1^T, \mathbf{d}_1^T, \mathbf{d}_2^T, \mathbf{b}_2^T, \mathbf{d}_3^T)^T$. Furthermore, stream *D2* is constrained to contain only the light key component methanol to guarantee a thermodynamically consistent distribution of the feed of column 2 to *D2* and *B2*. The feasibility of the splits in the three columns is ensured by nonlinear constraints based on the feasibility indicator m. Note that due to the placement of *D2* on the pure methanol vertex the feasibility of columns 1 and 3 implies that the split in column 2 is also feasible with respect to the distillation boundary. Hence, the feasibility constraint based on m_2 is omitted. In summary the model results to

$$\min \Phi_{En}(\mathbf{u}) = Q_{B1,\min}(\mathbf{u}) + Q_{B2,\min}(\mathbf{u}) + Q_{B3,\min}(\mathbf{u}) \quad (22)$$

$$\text{s.t} \quad m_{1,i} - d_{1,i} = b_{1,i}, \qquad i = 1, \ldots, C, \quad (23)$$

$$d_{1,i} - d_{2,i} = b_{2,i}, \qquad i = 1, \ldots, C, \quad (24)$$

$$b_{2,i} - d_{3,i} = b_{3,i}, \qquad i = 1, \ldots, C, \quad (25)$$

$$m_1(\mathbf{u}) \geq 1, \quad (26)$$

$$m_3(\mathbf{u}) \geq 1, \quad (27)$$

$$d_{2,\text{Ethanol}} = 0, \quad (28)$$

$$d_{2,\text{Water}} = 0, \quad (29)$$

$$u_j \geq 0, \qquad j = 1, \ldots, 5C. \quad (30)$$

A minimum overall reboiler heat duty $Q_{BT,\min} = 72.9$ MW is found with $Q_{B1,\min} = 35.2$ MW, $Q_{B2,\min} = 26.4$ MW, and

Table 3. Stream Table for the Ternary Curved Boundary Process with Three Columns at the Energetically Optimal Operating Point

Flow rate (kmol/s)	F	M1	D1	B1	D2	B2	D3	B3	M2
Methanol	0.000	0.273	0.273	0.000	0.273	0.000	0.000	0.000	0.273
Ethanol	0.040	0.061	0.061	0.000	0.000	0.061	0.021	0.040	0.021
Water	0.960	0.963	0.003	0.960	0.000	0.003	0.003	0.000	0.003
Total	1.000	1.297	0.337	0.960	0.273	0.064	0.024	0.040	0.297

$Q_{B3,min} = 11.3$ MW. The component flow rates at this operating point as obtained from $\mathbf{u}$ are given in Table 3.

Figure 11 presents a visualization of the mass balances of the process in a ternary diagram. The cutout gives a closer view of the location of $\mathbf{x}_{D1}$ and the course of the PDB. The distillate composition $\mathbf{x}_{D1}$ is located on the PDB close to the binary methanol–ethanol edge. Hence, the pinch points and rectification bodies of the first column in Figure 12 (left) show the characteristic tangent pinch situation (cf. first column of the ternary pressure swing separation in Figure 7, left). Contrarily, the second column displays regular feed pinch behavior (see Figure 12, right). The bottom product composition $\mathbf{x}_{B2}$ is located on the binary ethanol–water edge corresponding to a small recycle flow rate M_2 as could already be expected from the lever arm rule.

Eventhough the amount of water in *D1* is small, it is, however, still significant enough to make it impossible to obtain high-purity ethanol from column 2 directly. Hence, the binary separation in column 3 is mandatory for the final purification of the ethanol product. The energy demand of this relatively easy split is, however, small compared to the ones of columns 1 and 2. Considering the lever arm rule, it is evident that the separation effort required in column 3 is proportional to the distance of $\mathbf{x}_{D1}$ on the PDB to the binary methanol–ethanol edge. The need for the third column vanishes completely if $\mathbf{x}_{D1}$ touches this edge. Hence, the two-column process as shown in Figure 2b is obtained.

As can be inferred from the discussion above, the placement of $\mathbf{x}_{D1}$ is the crucial design decision for the two-column process. In this context, it is important to note the differences between SDB and PDB close to the binary methanol–ethanol edge. For high methanol concentrations, the SDB comes very close to the binary edge (see Figure 4). However, the SDB does not intersect the binary edge before reaching the pure methanol vertex. Hence, the SDB defines a minimum concentration of water in $\mathbf{x}_{D1}$ at $r \to \infty$ in a column with an infinite number of trays. In contrast to the SDB, the PDB intersects the binary edge at $\mathbf{x}_I = (0.929, 0.071, 0)$ well before reaching the pure methanol vertex (see cutout in Figure 11). Hence, it is theoretically possible to produce a product composition $\mathbf{x}_{D1,}$ which is essentially free of water in a reversible column with an unlimited number of trays. It can, therefore, be concluded that operation at limited reflux is superior to operation at infinite reflux for this specific split. This observation is contrary to the rule for the distillation of ideal mixtures stating that an increase in the reflux ratio will always improve the sharpness of a split.[25] Hence, this claim can not be extended to nonideal separations in all cases, even though it is treated as an universally valid rule by many authors. It should be noted, however, that in case of the mixture at hand the considerations presented above are of theoretical interest only. In practice, the

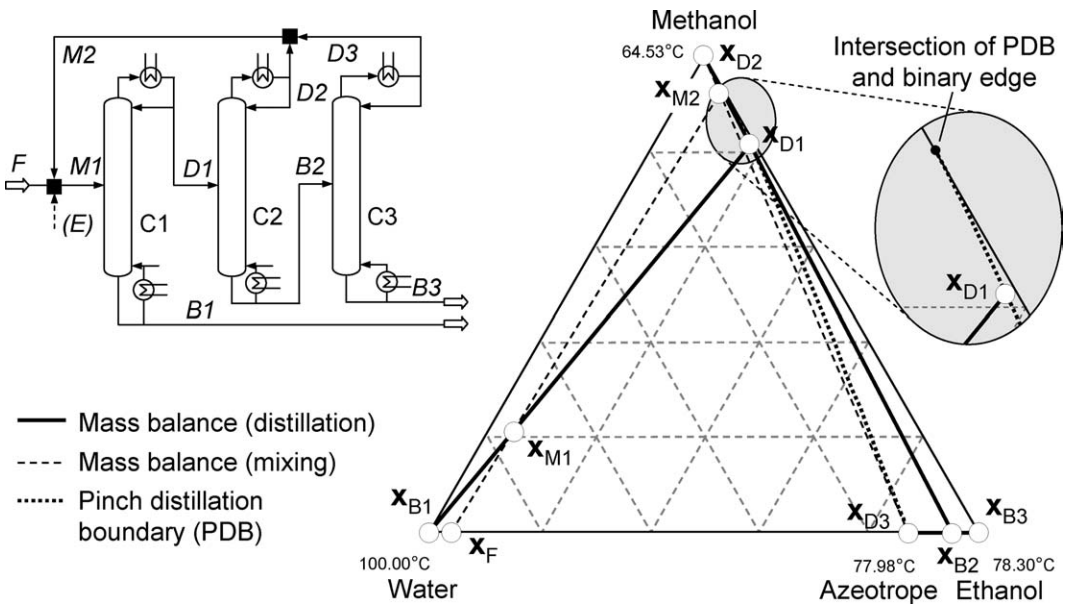

Figure 11. Mass balances of the ternary curved boundary process with three columns at the energetically optimal operating point.

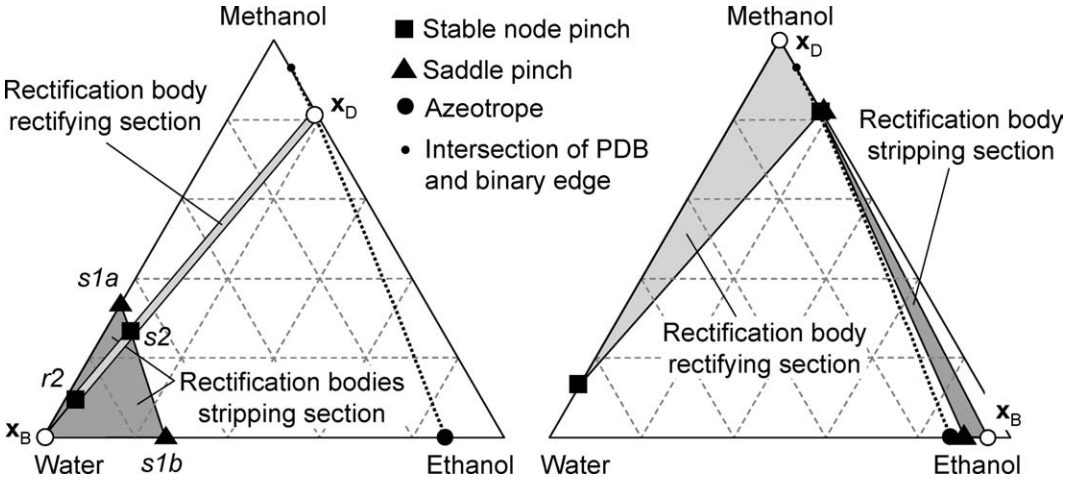

Figure 12. Rectification bodies of column 1 (left) and column 2 (right) at energy-optimal operating point and minimum energy demand.

first split will most likely be carried out in a column with a finite reflux and a relatively small number of trays. The effect of the limited number of trays which leads to the inclusion of impurities in $\mathbf{x}_{D1}$ will undoubtedly outmatch the influence of the reflux-dependency of the distillation boundary.

To obtain a cost estimate for the two-column process, the conceptual optimization model is formulated analogously to the one of the three-column process. Note that due to the smaller number of unit operations and streams only one degree of freedom is observed, namely the amount of methanol in stream *D1* which together with requiring feasibility of column 1 places $\mathbf{x}_{D1}$ between $\mathbf{x}_I$ and the pure methanol vertex. The energy-optimal operating point is found for $\mathbf{x}_{D1} = \mathbf{x}_I$ (see Table 4). A minimum overall reboiler heat duty $Q_{BT,min} = 99.1$ MW with $Q_{B1,min} = 46.0$ MW and $Q_{B2,min} = 53.1$ MW is obtained. Correspondingly, the two-column process requires 36% more heating steam than the three-column process. Hence, it is very likely to be economically inferior, even though it uses less equipment and, therefore, has lower investment cost.

Comparison of different objective functions

From a computational point of view, the minimization of the overall recycle flow rate Φ_{Rcy}, as opposed to the minimization of the overall reboiler heat duty addressed so far, has the attractive property that neither the RBM nor any other economic rating subroutine is necessary to evaluate the objective function. Hence, the computational effort is significantly reduced. To compare the results with the energy-based optimization, the three process examples discussed above, namely the two- and three-column ternary curved boundary processes and the ternary pressure-swing process, are recomputed with respect to the objective function

$$\min \Phi_{M1} = \sum_{j=1}^{C} m_{1,j}. \tag{31}$$

Note that Φ_{M1} addresses the minimization of the recycle flow rate indirectly. However, it is equivalent to a direct minimization of the recycle streams. The indirect formulation using Φ_{M1} has been chosen here because it can be equally applied to all process alternatives (see Figures 2a–c).

The recycle-optimized operating point of the three-column ternary curved boundary process is presented in Table 5. Comparison with Table 3 shows that the overall recycle flow rate has been reduced by 13% from 0.297 kmol/s to 0.258 kmol/s. The new operating point is characterized by a smaller amount of entrainer and a larger amount of water in stream D1. Table 6 compares the required minimum reboiler heat duties for both operating points. It can be seen that operation at the recycle-optimized operating point requires 11% more steam.

Quaternary curved boundary process

One of the most striking advantages of the screening framework based on PDB and RBM is that the conceptual optimization can be applied where simple graphical analysis fails, e.g., mixtures with more than three components. Consider a ternary feed mixture of two alcohols, namely ethanol and iso-propanol, and water (see Table 7 for compositions).

Table 4. Stream Table for the Ternary Curved Boundary Process with Two Columns at the Energetically Optimal Operating Point

Flow rate (kmol/s)	F	M1	D1	B1	D2	B2
Methanol	0.000	0.523	0.523	0.000	0.523	0.000
Ethanol	0.040	0.040	0.040	0.000	0.000	0.040
Water	0.960	0.960	0.000	0.960	0.000	0.000
Total	1.000	1.523	0.563	0.960	0.523	0.040

Table 5. Stream Table for the Ternary Curved Boundary Process with Three Columns at the Operating Point Corresponding to a Minimum Overall Recycle Flow Rate

Flow rate (kmol/s)	F	M1	D1	B1	D2	B2	D3	B3	M2
Methanol	0.000	0.205	0.205	0.000	0.205	0.000	0.000	0.000	0.205
Ethanol	0.040	0.086	0.086	0.000	0.000	0.086	0.046	0.040	0.046
Water	0.960	0.967	0.007	0.960	0.000	0.007	0.007	0.000	0.007
Total	1.000	1.258	0.298	0.960	0.205	0.093	0.053	0.040	0.258

Because of the relatively similar thermodynamic behavior of the two alcohols, they can be purified into one alcoholic product stream using the same three-column curved boundary process discussed above. The quaternary separation can be energy-optimized with the same model used for the ternary process given by Eqs. 22–30. However, the additional constraint

$$d_{3,\text{Propanol}} = 0, \tag{32}$$

is included to guarantee that the heaviest component isopropanol is completely removed in the bottom product of column 3.

The resulting energy-optimized operating point is shown in Table 7 and visualized in a quaternary phase diagram in Figure 13 (left). It can be seen that the additional iso-propanol–water azeotrope causes the formation of a planar two-dimensional PDB. Although it is barely visible from the graphs, this PDB is significantly curved. Analogously to the ternary process, the distillate composition $\mathbf{x}_{D1}$ of the first column is placed on the PDB. It is hard to see this from the mass balance in Figure 13 (left). However, it can be easily deduced from the appearance of the characteristic pitchfork bifurcation in the pinch map of the rectifying section of the first column which is shown in Figure 13 (right). The process has a minimum overall reboiler heat demand of $Q_{\text{BT,min}} = 101.3$ MW at the energy-optimized operating point. The heat duties of the individual columns are $Q_{\text{B1,min}} = 45.7$ MW, $Q_{\text{B2,min}} = 43.3$ MW and $Q_{\text{B3,min}} = 12.3$ MW, respectively. A comparison with the heat duties of the ternary process in Table 6 shows that the addition of the second alcohol results in an increase of the energy demand by 39%. Especially, the splits in the first two columns are significantly more demanding. This can partly be inferred from the respective rectification bodies shown in Figure 14. Analogously to the ternary separation, the first split of the quaternary process exhibits tangent pinch behavior due to a local maximum of the reflux ratio on the product pinch branch of the rectifying section at the pitchfork bifurcation. In contrast to the ternary separation, the second split of the quaternary process also shows tangent pinch behavior as can be seen from the overlapping of the bodies of the rectifying and stripping section in Figure 14 (right). The tangent pinch behavior is caused by a saddle-node bifurcation on the pinch branch of the rectifying section which runs on the binary methanol–ethanol edge. The limitation by this bifurcation must be overcome to obtain the saddle pinch on that edge. Similar to the ternary separation, the third split is characterized by a feed pinch. For the sake of brevity, the respective rectification bodies are not shown.

It is interesting to see that it is impossible to predict the impact of the addition of the second alcohol on the heat demand purely from considerations based on molecular similarity. On the one hand, the change from one single alcohol product, i.e., iso-propanol, to a mixture of ethanol and iso-propanol causes only a negligible increase in the heat duty of an extractive distillation process.[26] On the other hand, the heat demand increases significantly in case of the curved boundary process. Note that the calculations for both processes were performed using consistent thermodynamic data from the AspenPlus databanks. Hence, the different behavior can be exclusively attributed to the influence of the entrainers and the choice of the feed and product compositions.

Quaternary azeotropic purification without recycling

The different connectivity pattern of the PDB compared to the SDB (cf. first part of this series) is a very interesting phenomenon and holds important implications for process design. Consider the two-column curved boundary process discussed above (cf. Figure 4, right). The appearance of the intersection of the PDB with a binary edge is the key driver that facilitates the separation into high-purity products for this mixture. Note that in contrast to the three-column process, the two-column process does not involve any classical boundary-crossing split, i.e., a split where the product compositions and the feed lie in different distillation regions. Instead, the feed and the products of the first split are located exclusively in the water-rich distillation region, and the second column features a zeotropic binary mixture. However, a recycle stream is needed to manipulate the composition of the overall process feed such that this operating point can be attained. In this section, a different mixture consisting of acetone (A), chloroform (C), benzene (B), and toluene (T) is considered. It will be shown that a feed mixture containing all four components in non-negligible concentration can, under specific circumstances, be purified in three columns without introducing any recycle stream.

Table 6. Comparison of Minimum Reboiler Heat Duties at Different Operating Points

Operating point		min Φ_{Rcy}	min Φ_{En}
Recycle flow rate (kmol/s)	D_2	0.205	0.273
	D_3	0.053	0.024
	Total	0.258	0.297
Minimum reboiler heat duty (MW)	Column 1	40.8	35.2
	Column 2	21.4	26.4
	Column 3	18.6	11.3
	Total	80.8	72.9

Table 7. Stream Table for the Quaternary Curved Boundary Process with Three Columns (cf. Figure 2c) at the Energetically Optimal Operating Point

Flow rate (kmol/s)	F	M1	D1	B1	D2	B2	D3	B3	M2
Methanol	0.0000	0.4266	0.4266	0.0000	0.4259	0.0007	0.0007	0.0000	0.4266
Ethanol	0.0336	0.0668	0.0668	0.0000	0.0000	0.0668	0.0332	0.0336	0.0332
Iso-propanol	0.0084	0.0084	0.0084	0.0000	0.0000	0.0084	0.0000	0.0084	0.0000
Water	0.9580	0.9628	0.0048	0.9580	0.0000	0.0048	0.0048	0.0000	0.0048
Total	1.0000	1.4646	0.5066	0.9580	0.4259	0.0807	0.0387	0.0420	0.4646

To develop an understanding for the properties of the quaternary mixture ACBT, let us first take a look at the ternary submixture ACB in Figure 15 (left). The mixture exhibits a binary maximum azeotrope on the A-C edge. The azeotrope is the origin of a ternary distillation boundary. In case of the SDB (solid line), the boundary ends at the pure B vertex. Contrarily, the ternary part of the respective PDB (dotted line) ends at an intersection with the binary C-B edge at $x_C = 0.2085$. Furthermore, it can be shown that the addition of toluene does not form any new azeotropes and that the ternary submixture ACT behaves similarly to the ACB submixture. However, the intersection of the PDB with the binary C-T edge is found at $x_C = 0.1793$. Figure 15 (right) shows the resulting surface which represents the pinch distillation boundary of the quaternary mixture. It originates at the binary azeotrope. It terminates at the line describing its intersection with the ternary C-B-T face. Note that all compositions on the ternary face to the left of this line are accessible from the acetone-rich distillation region.

Consider an overall process feed $\mathbf{x}_F = (0.2, 0.15, 0.4, 0.25)$ of A, C, B and T, respectively, which is located in the acetone-rich distillation region. Two sharp splits can be conceived in this distillation region. The direct split is advantageous because it allows to obtain a high purity A product at the top of the first column C-1. Evaluation of the mass balance of this column shows that all A can be taken off such that the bottom product $\mathbf{x}_{B1}$ is located on the ternary C-B-T face to the left of the PDB line. As $\mathbf{x}_{B1}$ describes a ternary zeotropic mixture, it can be further purified in a sequence of two columns. Figure 15 (right) shows the respective mass balance for an indirect split removing T in column C-2 and a subsequent binary split between C and B in column C-3. Hence, a recycle stream is not needed. Contrarily, a process alternative without recycle streams cannot be found, if a feasibility analysis based on SDB[27] is used. Using successive examination of residue curves, it can be determined that the balance line of column C-1 intersects the SDB at $\mathbf{x}_I = (0.0105, 0.1855, 0.4948, 0.3092)$.

Hence, the bottom product *B1* is predicted to contain at least 1.05% A. This relatively small impurity may seem tolerable at first. However, the acetone in *B1* accumulates with the chloroform in the subsequent columns causing the final C product to contain a significant impurity of 5.4% A. Hence, the analysis of the SDB falsely suggest that high-purity C can only be obtained by introducing a boundary-crossing split and a recycle loop. This finding is also backed by other research groups who have published feasible column profiles originating from the binary benzene–chloroform edge (see Figure 5 of Lucia et al.[8]).

It is important to note that only a limited range of advantageous overall process feed compositions allows to devise a process alternative for the ACBT mixture which works without recycle streams. If the chloroform content in the feed is too high, it is not possible to access the ternary C-B-T face to the left of the PDB line. In such case, the introduction of a boundary-crossing split and a recycle loop indeed is imperative. Thong and Jobson[27] also suggest a large number of respective process alternatives with four columns. Note that in

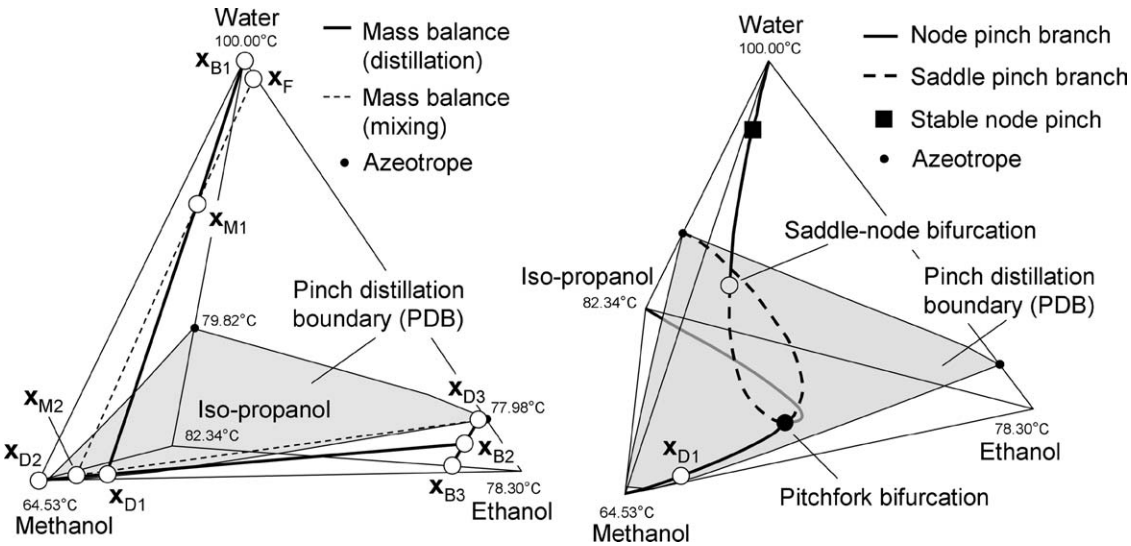

Figure 13. Mass balances of the quaternary curved boundary process with three columns at the energetically optimal operating point (left) and pinch map of the rectifying section of the first column (right).

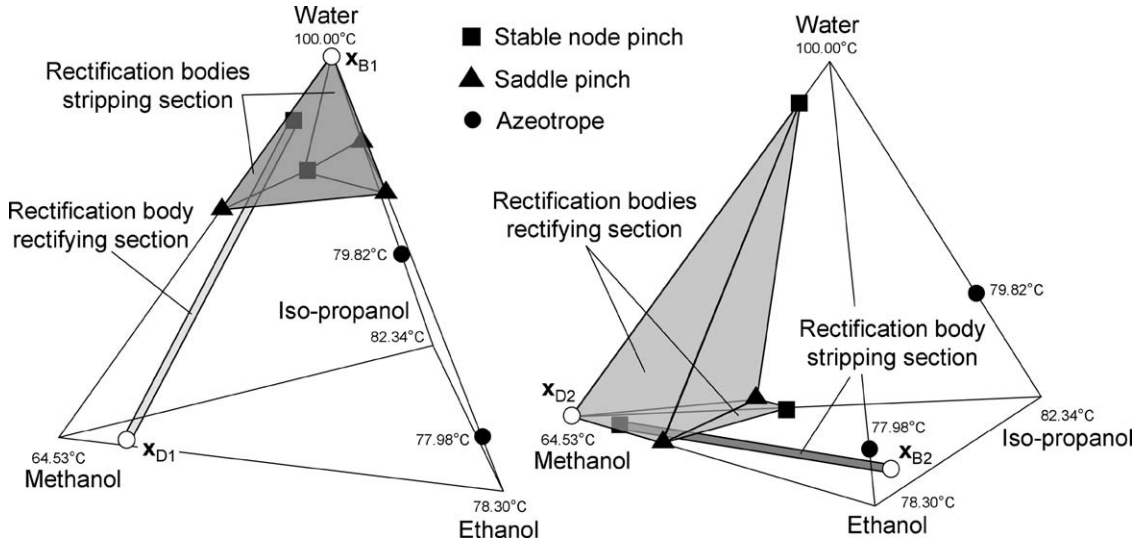

Figure 14. Rectification bodies of column 1 (left) and column 2 (right) at energy-optimal operating point and minimum energy demand.

addition process alternatives involving only three columns can be found using the same mechanisms as for the development of the two-column curved-boundary process from the three-column alternative. Whether this is economically attractive can, however, only be identified if the respective optimized operating points are compared using, for example, the procedure supplied in this article. For the sake of brevity, this will not be attempted here. A rigorous treatment of this mixture can be found elsewhere.[28]

Conclusions

In this article, the application of the new optimization-based design framework to the conceptual design of homogeneous processes with distillation boundaries has been presented. The formulation of the feasibility constraints imposed by the distillation boundaries in form of a nonlinear constraint to the optimization problem requires that a closed-form function $\mathbf{f}(\mathbf{x}) = \mathbf{0}$ describing the boundaries is known.

The feasibility constraints are based on the pinch distillation boundaries (PDB). The PDB approximates the real distillation boundaries by assuming a reversible distillation in each column.[21] In this case, the profile of the column is described by the pinch branches. Compositions on a distillation boundary are characterized by the appearance of a pitchfork bifurcation on these pinch branches. The calculation of the pitchfork bifurcation points, rules for the determination of the distillation boundaries and important properties of

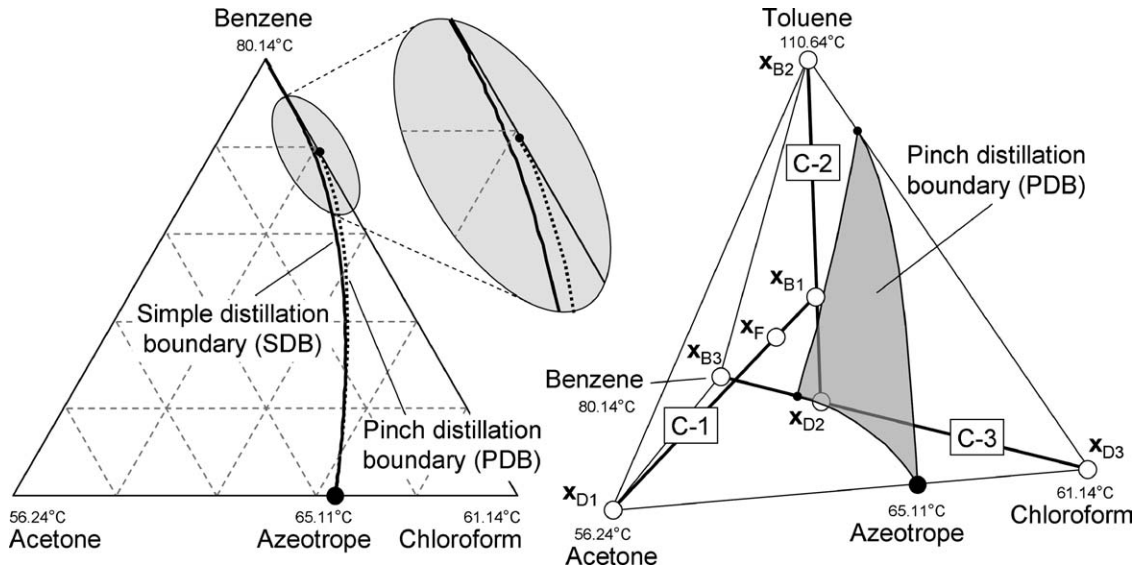

Figure 15. Simple distillation boundary (SDB) and pinch distillation boundary (PDB) of the ternary mixture acetone–chloroform–benzene at atmospheric pressure (left) and mass balances of the quaternary process without recycle streams (right).

these boundaries have been discussed in detail in the first article of this series.

A new, fully algorithmic feasibility test for the product composition of a column based on the PDB has been proposed. It does not require any graphical analysis and, therefore, is not limited by the number of components in the homogeneous mixture or the type of split. The feasibility test has been used within the new optimization-based design framework to determine the optimum operating point of the purification of ethanol in a pressure-swing process. The optimization of this operating point only needs a couple of CPU-minutes and runs completely without user intervention.

The successful application of the new design framework to additional ternary and quaternary examples further highlights the value of the bifurcation-based feasibility test. The PDB concept is based on a sound physical and mathematical definition and can be expected to provide a reasonably good approximation of the real distillation boundary even for complex multicomponent mixtures.

Within the scope of this article, the application of the design framework has been limited to the minimization of reboiler energy demand and recycle flowrates. A further refined screening objective can be achieved using a formulation for Φ that takes the dependency between energy cost and steam temperature into account. The thermodynamic efficiency η and the total energy cost are examples of such formulations. Using such objective functions, the new design framework can also be applied to find an optimized operating point for heat-integrated separation processes. Examples illustrating the influence of the formulation of the objective function on the location of the optimal operating point of the flowsheet are provided elsewhere.[10,24]

Literature Cited

1. Doherty MF, Malone MF. *Conceptual Design of Distillation Systems*. New York: McGraw-Hill, 2001.
2. Knapp JP, Doherty MF. A new pressure-swing-distillation process for separating homogeneous azeotropic mixtures. *Ind Eng Chem Res*. 1992;31:346–357.
3. Knight JR, Doherty MF. Optimal design and synthesis of homogeneous azeotropic distillation sequences. *Ind Eng Chem Res*. 1989;28:564–572.
4. Lucia A, Taylor R. The geometry of separation boundaries. I. Basic theory and numerical support. *AIChE J*. 2006;52:582–594.
5. Taylor R, Miller A, Lucia A. The geometry of separation boundaries: systems with reaction. *Ind Eng Chem Res*. 2006;45:2777–2786.
6. Bellows M, Lucia A. The geometry of separation boundaries: four component mixtures. *AIChE J*. 2007;53:1770–1778.
7. Lucia A, Taylor R. The geometry of separation boundaries. II. Mathematical formalism. *AIChE J*. 2006;53:1779–1788.
8. Lucia A, Amale A, Taylor R. Energy efficient hybrid separation processes. *Ind Eng Chem Res*. 2006;45:8319–8328.
9. Lucia A, Amale A, Taylor R. Distillation pinch points and more. *Comp Chem Eng*. 2008;32:1342–1364.
10. Brüggemann S. Rapid Screening of Conceptual Design Alternatives for Distillation Processes. PhD thesis Lehrstuhl für Prozesstechnik, RWTH Aachen in. Fortschrittberichte VDI, Reihe 3, Nr. 841, Düsseldorf, VDI Verlag, 2005.
11. Urdaneta RY, Bausa J, Brüggemann S, Marquardt W. Analysis and conceptual design of ternary heterogeneous azeotropic distillation processes. *Ind Eng Chem Res*. 2002;41:3849–3866.
12. Lewis WK. Dehydrating Alcohol and the Like. U.S. Pat. 1,676,700. July 10, 1928.
13. Black C. Distillation modeling of ethanol recovery and dehydration processes for ethanol and gasohol. *Chem Eng Prog*. 1980;76:78–85.
14. Stichlmair JG, Fair JR. *Distillation—Principles and Practices*. New York: Wiley-VCH, 1998.
15. Widagdo S, Seider WD. Azeotropic distillation. *AIChE J*. 1996; 42:96–130.
16. Bausa J, von Watzdorf R, Marquardt W. Shortcut methods for nonideal multicomponent distillation. I. Simple columns. *AIChE J*. 1998; 44:2181–2198.
17. Underwood AJ. Theory of phase equilibria in systems with multiple chemical reactions. *Chem Eng Prog*. 1948;44:603–614.
18. Levy SG, van Dongen DB, Doherty MF. Design and synthesis of homogeneous azeotropic distillations. II. Minimum reflux calculations for nonideal and azeotropic columns. *Ind Eng Chem Fundam*. 1985;24:463–474.
19. Bausa J. Näherungsverfahren für den konzeptionellen Entwurf und die thermodynamische Analyse von destillativen Trennprozessen. PhD thesis Lehrstuhl für Prozesstechnik, RWTH Aachen in. Fortschrittberichte VDI, Reihe 3, Nr. 692. Düsseldorf, VDI Verlag, 2001.
20. Julka V, Doherty MF. Geometric behavior and minimum flows for nonideal multicomponent distillation. *Chem Eng Sci*. 1990;45: 1801–1822.
21. Köhler J, Aguirre P, Blass E. Minimum reflux calculations for nonideal mixtures using the reversible distillation model. *Chem Eng Sci*. 1991;49:3325–3330.
22. Pöllmann P, Glanz SB, Blass E. Calculating minimum reflux of nonideal multicomponent distillation using eigenvalue theory. *Comp Chem Eng*. 1994;18(S):S49–S53.
23. Lawrence CT, Tits AL. A computationally efficient feasible sequential quadratic programming algorithm. *SIAM J Opt*. 2001;11:1092–1118.
24. Brüggemann S, Marquardt W. Rapid screening of design alternatives for nonideal multiproduct distillation processes. *Comp Chem Eng*. 2005;29:165–179.
25. King CJ. *Separation Processes*. New York: McGraw-Hill, 1980.
26. Brüggemann S, Marquardt W. Shortcut methods for nonideal multicomponent distillation. III. Extractive distillation columns. *AIChE J*. 2004;50:1129–1149.
27. Thong, DY, Jobson M. Multicomponent homogeneous azeotropic distillation. III. Column sequence synthesis. *Chem Eng Sci*. 2001; 56:4417–4432.
28. Kraemer K, Kossack S, Marquardt W. Efficient optimization-based design of distillation processes for homogeneous azeotropic mixtures. *Ind Eng Chem Res*. 2009;48:6749–6764.

Manuscript received July 30, 2007, revision received May 25, 2010, and final revision received July 10, 2010.